1

2

3 **A robust Upwind Mixed Hybrid Finite Element method for transport**

4 **in variably saturated porous media**

5
6
7
8 Anis Younes[1*], Hussein Hoteit[2], Rainer Helmig[3], Marwan Fahs[1]

9

10 [1] Institut Terre et Environnement de Strasbourg, Université de Strasbourg, CNRS, ENGEES, UMR 7063, 67084

11 Strasbourg, France

12 [2] Physical Science and Engineering Division, King Abdullah University of Science and Technology (KAUST),
13 Thuwal, Saudi Arabia
14 [3] Institute for Modelling Hydraulic and Environmental Systems, University of Stuttgart, Pfaffenwaldring 61,
15 70569 Stuttgart, Germany
16
17
18
19
20
21
22
23
24
25
26

27 Contact author: Anis Younes

28 E-mail: younes@unistra.fr

29

30

31

32

33

34

35

36

37

38

## Abstract

40  The Mixed Finite Element (MFE) method is well adapted for the simulation of fluid flow in

41  heterogeneous porous media. However, when employed for the transport equation, it can

42  generate solutions with strong unphysical oscillations because of the hyperbolic nature of

43  advection. In this work, a robust upwind MFE scheme is proposed to avoid such unphysical

44  oscillations. The new scheme is a combination of the upwind edge/face centred finite volume

45  method with the hybrid formulation of the MFE method. The scheme ensures continuity of

46  both advective and dispersive fluxes between adjacent elements and allows to maintain the

47  time derivative continuous, which permits employment of high order time integration

48  methods via the Method of Lines (MOL).

49  Numerical simulations are performed in both saturated and unsaturated porous media to

50  investigate the robustness of the new upwind-MFE scheme. Results show that, contrarily to

51  the standard scheme, the upwind-MFE method generates stable solutions without under and

52  overshoots. The simulation of contaminant transport into a variably saturated porous medium

53  highlights the robustness of the proposed upwind scheme when combined with the MOL for

54  solving nonlinear problems.

55

56  *Keywords*:

57  Hybrid Mixed Finite Element, upwind scheme, advection-dispersion transport, numerical

58  oscillations, Method of Lines.

59

60

## 1. Introduction

The Mixed Finite Element (MFE) method (Raviart and Thomas, 1977; Brezzi *et al.*, 1985; Chavent and Jaffré, 1986; Brezzi and Fortin, 1991, Younes *et al.*, 2010) is known to be a robust numerical scheme for solving elliptic diffusion problems such as the fluid flow in heterogeneous porous media. The method combines advantages of the finite volumes, by ensuring local mass conservation and continuity of fluxes between adjacent cells, and advantages of finite elements by easily handling heterogeneous domains with discontinuous parameter distributions and unstructured meshes. As a consequence, the MFE method has been largely used for flow in porous media (see, for instance, the review of Younes *et al*. (2010) and references therein). The hybridization technique has been largely used with the MFE method to improve its efficiency (Chavent and Roberts, 1991; Traverso *et al*. 2013). This technique allows to reduce the total number of unknowns and produces a final system with a symmetric positive definite matrix. The unknowns with the hybrid-MFE method are the Lagrange multipliers which correspond to the traces of the scalar variable at edges/faces (Chavent and Jaffré, 1986).

When applied to transient diffusion equations with small time steps, the hybrid-MFE method can produce solutions with small unphysical over and undershoots (Hoteit *et al*., 2002a, 2002b; Mazzia, 2008). A lumped formulation of the hybrid-MFE method was developed by Younes *et al.* (2006) to improve its monotonicity and reduce nonphysical oscillations. The lumped formulation ensures that the maximum principle is respected for parabolic diffusion equations on acute triangulations (Younes *et al.*, 2006). For more general 2D and 3D element shapes, the lumping procedure allows to significantly improve the monotonous character of the hybrid-MFE solution (Younes *et al*., 2006; Koohbor *et al.*, 2020). As an illustration, the lumped formulation was shown to be more efficient and more robust than the standard hybrid formulation for the simulation of the challenging nonlinear problem of water infiltration into

3

86    an initially dry soil (Belfort *et al*., 2009). The lumped formulation has recently been used for

87    flow discretization in the case of density driven flow in saturated-unsaturated porous media

88    (Younes *et al*., 2022a).

89    However, the MFE method remains little used for the discretization of the full transport

90    equation. When employed to the advection-dispersion equation, the MFE method can

91    generate solutions with strong numerical instabilities in the case of advection-dominated

92    transport because of the hyperbolic nature of the advection operator. To avoid these

93    instabilities, one of the most popular and easiest ways is to use an upwind scheme. Indeed,

94    although upwind schemes introduce some numerical diffusion leading to an artificial

95    smearing of the numerical solution, they avoid unphysical oscillations and remain useful,

96    especially for large domains and regional field simulations. In the literature, some upwind

97    mixed finite element schemes have been employed to improve the robustness of the MFE

98    method for advection-dominated problems (Dawson, 1998; Dawson and Aizinger, 1999;

99    Radu *et al*., 2011; Vohralik, 2007; Brunner *et al*., 2014).

100   The main idea of an upwind scheme for an element $E$, is to calculate the mass flux exchanged

101   with its adjacent element $E$' using the concentration from $E$ in the case of an outflow and the

102   concentration from $E'$ in the case of an inflow. However, this idea cannot be applied as such

103   with the hybrid-MFE method since the hybridization procedure requires to express the flux at

104   the element interface as only a function of variables at the element $E$ (and not $E$'). To

105   overcome this difficulty, Radu *et al.* (2011), and Brunner *et al.* (2014) proposed an upwind

106   MFE method where, in the case of an inflow, the concentration at the adjacent element $E$' is

107   replaced by an approximation using the concentration at $E$ and the trace of concentration at

108   the interface $\partial_{EE'}$ by assuming that the edge concentration is the mean of the concentrations in

109   $E$ and $E$'. However, this assumption cannot be verified for a general configuration.

110  Furthermore, with such an assumption, each of the advective and dispersive fluxes is

111  discontinuous at the element interfaces, and continuity is only fulfilled for the total flux.

112  In this work, a new upwind-MFE method is proposed for solving the full transport equation

113  without requiring any approximation of the upwind concentration. The new scheme is a

114  combination of the upwind edge/face centered finite volume (FV) scheme with the lumped

115  formulation of the MFE method. It guarantees continuity of both advective and dispersive

116  fluxes at element interfaces. Further, the new upwind-MFE scheme maintains the time

117  derivative continuous and thus, allows to employ high order time integration methods via the

118  method of lines (MOL), which was shown to be very efficient for solving nonlinear problems

119  (see, for instance, Fahs *et al*. (2009) and Younes *et al*. (2009)).

120  This article is structured as follows. In section 2, we recall the hybrid-MFE method for the

121  discretization of the transport equation. In section 3, we introduce the new upwind-MFE

122  method based on the combination of the upwind edge/face FV scheme with the lumped

123  formulation of the MFE method. In section 4, numerical experiments are performed for

124  transport in saturated and unsaturated porous media to investigate the robustness of the new

125  developed upwind-MFE scheme. Some conclusions are given in the last section of the article.

## 2. The hybrid-MFE method for the advection-dispersion equation

126

127  The mass conservation of the contaminant in variably saturated porous media is:

128
$$\frac{\partial(\theta C)}{\partial t} + \nabla.\left(\tilde{\boldsymbol{q}}_a + \tilde{\boldsymbol{q}}_d\right) = 0 \tag{1}$$

129  where $C$ is the normalized concentration [-], $\theta$ is water content [$L^3 L^{-3}$], ], $t$ is time [T],

130  $\tilde{\boldsymbol{q}}_a = \boldsymbol{q}C$ is the advective flux with $\boldsymbol{q}$ the Darcy velocity [$LT^{-1}$] and $\tilde{\boldsymbol{q}}_d$ the dispersive flux

131  given by:

132
$$\tilde{\boldsymbol{q}}_d = -\boldsymbol{D}\nabla C \tag{2}$$

133  with $\boldsymbol{D}$, the dispersion tensor, expressed by:

134 $$\boldsymbol{D} = D_m\boldsymbol{I} + \left(\alpha_L - \alpha_T\right)\boldsymbol{q} \otimes \boldsymbol{q} / |\boldsymbol{q}| + \alpha_T |\boldsymbol{q}|\boldsymbol{I} \tag{3}$$

135 in which $\alpha_L$ and $\alpha_T$ are the longitudinal and transverse dispersivities [L], $D_m$ is the pore

136 water diffusion coefficient [$L^2T^{-1}$] and $\boldsymbol{I}$ is the unit tensor.

137 The water content $\theta$ and the Darcy velocity $\boldsymbol{q}$ are linked by the fluid mass conservation

138 equation in variably saturated porous media:

139 $$\frac{\partial \theta}{\partial t} + \nabla.\,\boldsymbol{q} = 0 \tag{4}$$

140 Substituting Eq. (4) into Eq. (1) yields the following advection-dispersion equation:

141 $$\theta\frac{\partial C}{\partial t} + \nabla.\left(\tilde{\boldsymbol{q}}_a + \tilde{\boldsymbol{q}}_d\right) - C\nabla.\boldsymbol{q} = 0 \tag{5}$$

142 In this work, we consider that the velocity $\boldsymbol{q}$ is obtained by solving Richards' equation using

143 the hybrid-MFE method. For a two-dimensional domain with a triangular mesh, $\boldsymbol{q}$ is

144 approximated inside each triangle $E$ using the lowest-order Raviart-Thomas (RT0) vectorial

145 basis functions $\boldsymbol{w}_j^E$:

146 $$\boldsymbol{q} = \sum_{j=1}^{3} Q_j^E \boldsymbol{w}_j^E \tag{6}$$

147 where $Q_j^E$ is the water flux across the edge $E_j$ of $E$ (see Figure 1) and $\boldsymbol{w}_j^E = \dfrac{1}{2|E|}\begin{pmatrix} x - x_j^E \\ y - y_j^E \end{pmatrix}$

148 is the typical RT0 basis functions (Younes *et al.*, 1999) with $\left(x_j^E, y_j^E\right)$ the coordinates of the

149 node $j$ opposite to the edge $E_j$ of $E$ and $|E|$, the area of $E$.
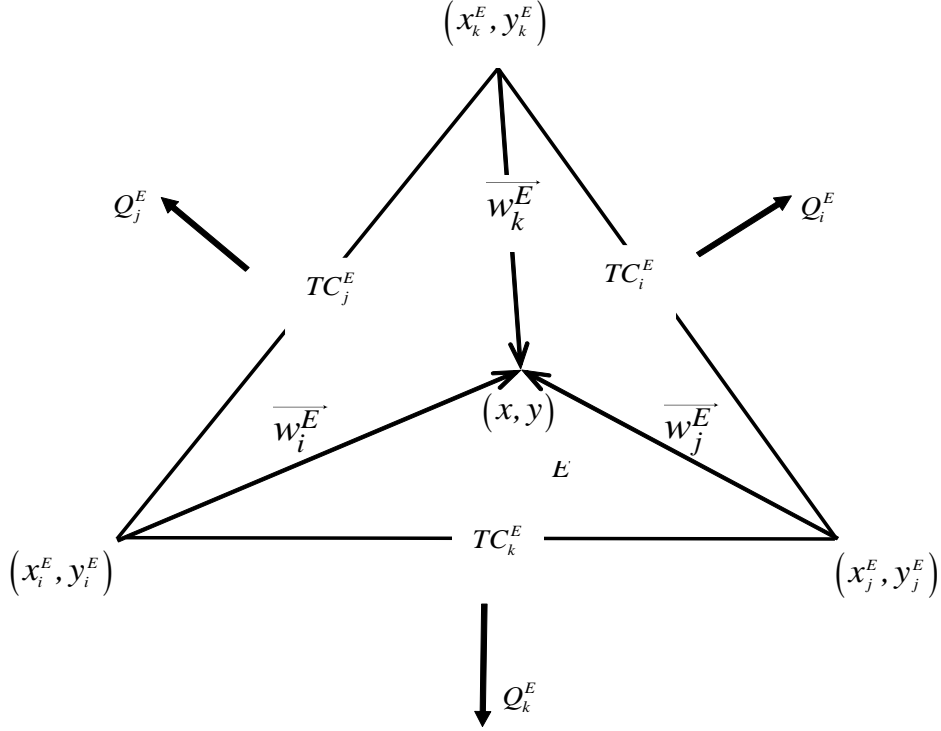
Figure 1: Vectorial basis functions for the MFE method.

To apply the hybrid-MFE method to the transport Eq. (5), we approximate the dispersive flux $\tilde{\boldsymbol{q}}_d$ with RT0 vectorial basis functions as:

$$\tilde{\boldsymbol{q}}_d = \sum_{j=1}^{3} \tilde{Q}_j^{d,E} \boldsymbol{w}_j^E \tag{7}$$

where $\tilde{Q}_j^{d,E} = \int_{E_j} \tilde{\boldsymbol{q}}_d . \boldsymbol{\eta}_j^E$ is the dispersive flux across the edge $E_j$ of the element $E$ and $\boldsymbol{\eta}_j^E$ is

the outward unit normal vector to the edge $E_j$.

The variational formulation of Eq. (2) using the test function $\boldsymbol{w}_i^E$ yields:

$$\int_E \boldsymbol{D}^{-1} \tilde{\boldsymbol{q}}_d \boldsymbol{w}_i^E = \int_E C\nabla . \boldsymbol{w}_i^E - \sum_j \int_{E_j} C\boldsymbol{w}_i^E . \boldsymbol{\eta}_j^E \tag{8}$$

Substituting Eq. (7) into Eq. (8) and using properties of the basis functions $\boldsymbol{w}_j^E$ give

161

$$\sum_j \tilde{Q}_j^{d,E} \int_E \left( \boldsymbol{D}_E^{-1} \boldsymbol{w}_j^E \right).\boldsymbol{w}_i^E = \frac{1}{|E|}\int_E C - \frac{1}{|E_i|}\int_{E_i} C \tag{9}$$

$$= C_E - TC_i^E$$

162 in which, $\boldsymbol{D}_E$ is the local dispersion tensor at the element $E$, $C_E$ is the mean concentration at

163 $E$ and $TC_i^E$ is the edge (trace) concentration (Lagrange multiplier) at the edge $E_i$.

164 Denoting the local matrix $\tilde{B}_{i,j}^E = \int_E \left( \boldsymbol{D}_E^{-1} \boldsymbol{w}_j^E \right).\boldsymbol{w}_i^E$, the inversion of the system of Eq. (9) gives

165 the expression for the dispersive flux $\tilde{Q}_i^{d,E}$:

$$\tilde{Q}_i^{d,E} = \sum_j \tilde{B}_{i,j}^{E,-1} \left( C_E - TC_j^E \right) \tag{10}$$

167 Besides, the integration of the mass conservation Eq. (6) over the element $E$ writes

$$\int_E \theta \frac{\partial C}{\partial t} + \int_E \nabla.\tilde{\boldsymbol{q}}_a + \int_E \nabla.\tilde{\boldsymbol{q}}_d - \int_E C\nabla.\boldsymbol{q} = 0 \tag{11}$$

169 which becomes, using Green's formula,

$$\theta_E |E| \frac{\partial C_E}{\partial t} + \sum_i \int_{E_i} C\boldsymbol{q}.\boldsymbol{\eta}_i^E + \sum_i \int_{E_i} \tilde{\boldsymbol{q}}_d.\boldsymbol{\eta}_i^E - \int_E C\nabla.\boldsymbol{q} = 0 \tag{12}$$

171 where $\theta_E$ is the water content of the element $E$.

172 Substituting Eq. (2) into Eq. (12) yields

$$\theta_E |E| \frac{\partial C_E}{\partial t} + \sum_i \underbrace{\left( \tilde{Q}_i^{a,E} + \tilde{Q}_i^{d,E} \right)}_{\tilde{Q}_i^{t,E}} - C_E \sum_i Q_i^E = 0 \tag{13}$$

174 in which $\tilde{Q}_i^{t,E} = \tilde{Q}_i^{a,E} + \tilde{Q}_i^{d,E}$ is the total flux at the edge $E_i$ with $\tilde{Q}_i^{a,E}$ the advective flux given

175 by $\tilde{Q}_i^{a,E} = Q_i^E TC_i^E$ and $\tilde{Q}_i^{d,E}$ the dispersive flux given by Eq. (10).

176 The hybridization of the MFE method is performed in the following two steps:

177 1) The flux Eq. (10) is substituted into the mass conservation Eq. (13), which is then

178     discretized in time using the first-order implicit Euler scheme

179 $$\theta_E \frac{|E|}{\Delta t}\left(C_E^{n+1} - C_E^{n}\right) + \sum_i Q_i^E TC_i^{E,n+1} - C_E^{n+1}\sum_i Q_i^E + \tilde{\alpha}^E C_E^{n+1} - \sum_i \tilde{\alpha}_i^E TC_i^{E,n+1} = 0 \qquad (14)$$

180 in which $\tilde{\alpha}_i^E = \sum_j \tilde{B}_{i,j}^{E,-1}$ and $\tilde{\alpha}^E = \sum_i \tilde{\alpha}_i^E$.

181 Hence, the mean concentration at the new time level $C_E^{n+1}$ can be expressed as a function

182 of $TC_i^{E,n+1}$, the concentration at the edges of $E$, as follows:

183 $$C_E^{n+1} = \frac{1}{\beta_E}\sum_i \left(\tilde{\alpha}_i^E - Q_i^E\right)TC_i^{E,n+1} + \frac{\lambda_E}{\beta_E}C_E^{n} \qquad (15)$$

184 in which $\lambda_E = \theta_E \frac{|E|}{\Delta t}$ and $\beta_E = \left(\lambda_E + \tilde{\alpha}^E - \sum_i Q_i^E\right)$.

185 The mean concentration given by Eq. (15) is then substituted into the flux Eq. (10), which

186 allows expressing the dispersive flux $\tilde{Q}_i^{d,E,n+1}$ (the subscript n+1 will be omitted to alleviate

187 the notations) as only a function of the traces of concentration at edges $TC_i^{E,n+1}$:

188 $$\tilde{Q}_i^{d,E} = \sum_j \left(\frac{\tilde{\alpha}_i^E}{\beta_E}\left(\tilde{\alpha}_j^E - Q_j^E\right) - \tilde{B}_{i,j}^{E,-1}\right)TC_j^{E,n+1} + \frac{\lambda_E}{\beta_E}\tilde{\alpha}_i^E C_E^{n} \qquad (16)$$

189 2) The system to be solved is obtained by imposing the continuity of the total flux

190 $\left(\tilde{Q}_i^{t,E} + \tilde{Q}_i^{t,E'} = 0\right)$ as well as the continuity of the trace of concentration $\left(TC_i^{E,n+1} = TC_i^{E',n+1}\right)$

191 at the edge $i$ between the two elements $E$ and $E'$ (Figure 2).
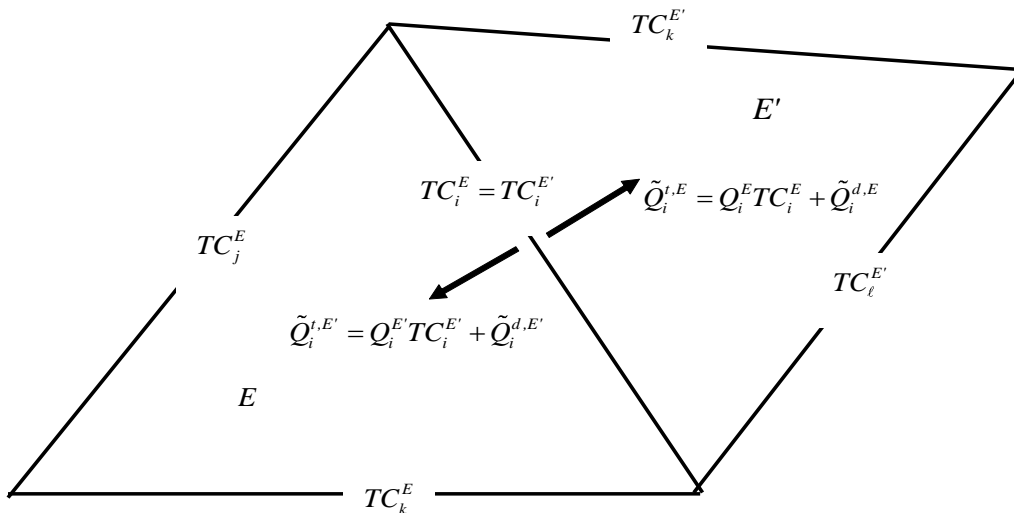
192

193    Figure 2: Continuity of concentration and total flux between adjacent elements with the

194                                    hybrid-MFE method.

195    Note that the advective flux $\tilde{Q}_i^{a,E}$ is continuous between $E$ and $E'$ because of the continuity

196    of the water flux and the continuity of the trace of concentration at the interface. Thus, for

197    the continuity of the total flux $\left( \tilde{Q}_i^{t,E} + \tilde{Q}_i^{t,E'} = 0 \right)$, it is required that the dispersive flux is

198    continuous:

199
$$\tilde{Q}_i^{t,E} + \tilde{Q}_i^{t,E'} = \left( Q_i^E + Q_i^{E'} \right) TC_i^{E,n+1} + \tilde{Q}_i^{d,E} + \tilde{Q}_i^{d,E'} = \tilde{Q}_i^{d,E} + \tilde{Q}_i^{d,E'} = 0 \tag{17}$$

200    Using Eq. (16), we obtain:

201
$$\sum_j \left( \tilde{B}_{i,j}^{E,-1} - \frac{\tilde{\alpha}_i^E}{\beta_E} \left( \tilde{\alpha}_j^E - Q_j^E \right) \right) TC_j^{E,n+1} + \sum_j \left( \tilde{B}_{i,j}^{E',-1} - \frac{\tilde{\alpha}_i^{E'}}{\beta_{E'}} \left( \tilde{\alpha}_j^{E'} - Q_j^{E'} \right) \right) TC_j^{E',n+1}$$
$$= \frac{\lambda_E}{\beta_E} \tilde{\alpha}_i^E C_E^{\,n} + \frac{\lambda_{E'}}{\beta_{E'}} \tilde{\alpha}_i^{E'} C_{E'}^{\,n} \tag{18}$$

202    The continuity Eq. (18) is written for all mesh edges, and the resulting equations form the

203    final system to be solved for the traces of concentration at edges $TC_i^{E,n+1}$ as unknowns.

204    Note that the hybrid-MFE Eqs (18), obtained by approximating the dispersive flux with RT0

205    basis functions, is equivalent to the new MFE method proposed in Radu *et al*. (2011).


## 3. The upwind and lumped MFE approaches

207    In this section, we recall the main principles of two existing approaches, developed to

208    improve the stability of the MFE solution of the transport equation. The first approach is the

209    upwind-hybrid MFE scheme of Radu et al. (2011), developed for advection dominated

210    transport. The second approach is the lumped hybrid-MFE method of Younes *et al.* (2006),

211    developed for dispersive transport.

### 3.1 The upwind-hybrid MFE of Radu et al. (2011)

213

214    In the case of advection-dominated transport, solving the hybrid-MFE Eq. (18) can yield

215    solutions with strong instabilities. A common way to avoid such instabilities is to use an

216    upwind scheme for the advective flux. Thus, for an element $E$, the advective flux

217    $\tilde{Q}_i^{a,E} = Q_i^E TC_i^E$ at the edge $i$ (common with the element $E$'), has to be calculated using either

218    the concentration from $E$ (if $Q_i^E > 0$) or the concentration from $E$' (if $Q_i^E < 0$). Radu *et al.*

219    (2011) suggested replacing the advective flux $\tilde{Q}_i^{a,E} = Q_i^E TC_i^E$ at the interface by:

$$220 \qquad \tilde{Q}_i^{a,E} = \begin{cases} Q_i^E C^E & if & Q_i^E > 0 \\ Q_i^E C^{E'} & if & Q_i^E < 0 \end{cases} \qquad (19)$$

221    The advective term is now calculated using the upwind mean concentration, which can be that

222    of the element $E$ or of its adjacent element $E$'.

223    The advective flux of Eq. (19) is rewritten in the following condensed form

$$224 \qquad \tilde{Q}_i^{a,E} = Q_i^E \left( \tau_i^E C^E + \left(1 - \tau_i^E\right) C^{E'} \right) \qquad (20)$$

225    with $\tau_i^E = 1$ for an outflow $\left(Q_i^E > 0\right)$ and $\tau_i^E = 0$ for an inflow $\left(Q_i^E < 0\right)$.

226    However, this expression is incompatible with the hybridization procedure. Indeed, if we

227    replace, in the Eq. (14), the advective term $Q_i^E TC_i^E$ by Eq. (20), the latter will contain both

228    $C^E$ and $C^{E'}$. Thus, the first step of the hybridization procedure cannot allow expressing

229    $C_E^{n+1}$ as only a function of $TC_i^{E,n+1}$ as in the Eq. (15).

230    To avoid this difficulty, Radu *et al.* (2011) suggested replacing, $C^{E'}$ by the following

231    expression:

$$232 \qquad C^{E'} \simeq 2TC_i^E - C^E \qquad (21)$$

233    This approximation is based on the assumption that $TC_i^E \simeq \left(C^E + C^{E'}\right)/2$.

234    Plugging Eq. (21) into Eq. (20), the advective flux $\tilde{Q}_i^{a,E}$ depends only on the variables of the

235    element $E$ (mean concentration $C^E$ and edge concentration $TC_i^E$):

11

236
$$\tilde{Q}_i^{a,E} = Q_i^E \left( \tau_i^E C^E - \left(1 - \tau_i^E\right) C^E + 2\left(1 - \tau_i^E\right) TC_i^E \right)$$ (22)

237 Eq. (22) can then be used to replace the advective term $Q_i^E TC_i^{E,n+1}$ in Eq. (14), and thus the

238 hybridization procedure allows to express $C_E^{n+1}$ as a function of $TC_i^{E,n+1}$ as in the Eq. (15).

239 Then, the expression of $C_E^{n+1}$ is substituted into the dispersive flux Eq. (10), and the final

240 system is obtained by prescribing continuity of the total flux $\left( \tilde{Q}_i^{t,E} + \tilde{Q}_i^{t,E'} = 0 \right)$ at the interface

241 between $E$ and $E'$. This scheme was shown to be more efficient (by using a sparser system

242 matrix with fewer unknowns) than the non-hybrid upwind mixed method of Dawson (1978).

243 The two methods yielded optimal first order convergence in time and space (Brunner *et al.*,

244 2014).

245 The assumption given by Eq. (21) can be a rough approximation, especially in the case of a

246 heterogeneous domain where dispersion can vary with several orders of magnitudes from

247 element to element. For such a situation, the edge concentration can be significantly different

248 from the average of the mean concentrations of adjacent elements. Furthermore, the advective

249 flux is not uniquely defined at the interface and can be different for the two adjacent elements

250 $E$ and $E'$. For instance, in the case of $Q_i^E = Q > 0$, the advective flux leaving the element $E$ is

251 $\tilde{Q}_i^{a,E} = QC^E$, whereas the flux entering the element $E'$ is $\tilde{Q}_i^{a,E'} = Q\left(2TC_i^E - C^{E'}\right)$ which could

252 be different as $TC_i^E$ is not necessarily the mean of $C^E$ and $C^{E'}$. In this situation, because of

253 the discontinuity of the advective flux, the dispersive flux will not be continuous at the

254 interface since the continuity is prescribed only for the total flux.

255 **3.2 The lumped hybrid-MFE scheme for dispersion transport**

256 In this section, we recall the main principles of the lumped hybrid-MFE method of Younes *et*

257 *al.* (2006), developed to improve the stability of the MFE solution in the case of dispersive

258 transport.

259     Considering only dispersion, Eq. (5) simplifies to:

$$\theta \frac{\partial C}{\partial t} + \nabla . \tilde{\boldsymbol{q}}_d = 0 \tag{23}$$

261     As detailed above, the hybrid MFE method for Eq. (23) is based on two stages:

262     • *Stage1: discretization of the transient mass conservation equation over the element E:*

263     The integration of the mass conservation Eq. (23) over the element $E$ gives (see Eq.

264     13):

$$\theta_E |E| \frac{\partial C_E}{\partial t} + \sum_i \tilde{Q}_i^{d,E} = 0 \tag{24}$$

266     • *Stage2: imposing the continuity of the flux across the edge i sharing the two elements*

267     *E and E':*

$$\tilde{Q}_i^{d,E} + \tilde{Q}_i^{d,E'} = 0 \tag{25}$$

269     Note that the continuity equation (25) can be interpreted as a steady state mass conservation

270     equation at the edge level. Hence, the hybrid MFE discretization uses the transient mass

271     conservation equation at the element level, given by Eq. (24), and the steady state mass

272     conservation at the edge level, given by Eq. (25). With the lumped hybrid MFE method of

273     Younes *et al.* (2006), the transient term is taken into account at the edge level. Hence, the

274     lumped formulation uses a steady state mass conservation equation at the element level and a

275     transient mass conservation equation at the edge level. The two stages of the lumped hybrid

276     MFE are as follows:

277     • *Stage1: discretization of the steady-state mass conservation equation over E:*

278     The steady-state transport over the element $E$ writes:

$$\sum_i \tilde{\underline{Q}}_i^{d,E} = 0 \tag{26}$$

280     where $\tilde{\underline{Q}}_i^{d,E}$ is the steady-state dispersive flux across the edge $E_i$.

281     Therefore, the mean concentration of Eq. (15) becomes

282
$$C_E = \sum_i \frac{\tilde{\alpha}_i^E}{\tilde{\alpha}^E} TC_i^E \qquad (27)$$

283     and using Eq. (16), the steady-state dispersive flux writes

284
$$\underline{\tilde{Q}}_i^{d,E} = \sum_j \left( \frac{\tilde{\alpha}_i^E \tilde{\alpha}_j^E}{\tilde{\alpha}^E} - \tilde{B}_{i,j}^{E,-1} \right) TC_j^E \qquad (28)$$

285     • *Stage2: discretization of the transient mass conservation equation over the lumping*

286        *region* $R_i$

287     The edge centered finite volume discretization of the transient transport Eq. (23) over

288     the lumping region $R_i$ (hatched area in Figure 3), associated with the edge $i$, writes:

289
$$\int_{R_i} \theta \frac{\partial C}{\partial t} + \int_{R_i} \nabla . \tilde{q}_d = 0 \qquad (29)$$

290     where the lumping regions $R_i$ is formed by the two simplex regions $S_i^E$ and $S_i^{E'}$, for

291     an inner edge $i$ sharing the two elements $E$ and $E'$, and by the sole simplex region

292     $S_i^E$ for a boundary edge. The simplex region $S_i^E$ is defined by joining the centre of $E$

293     with the nodes *j* and *k* forming the edge *i*.
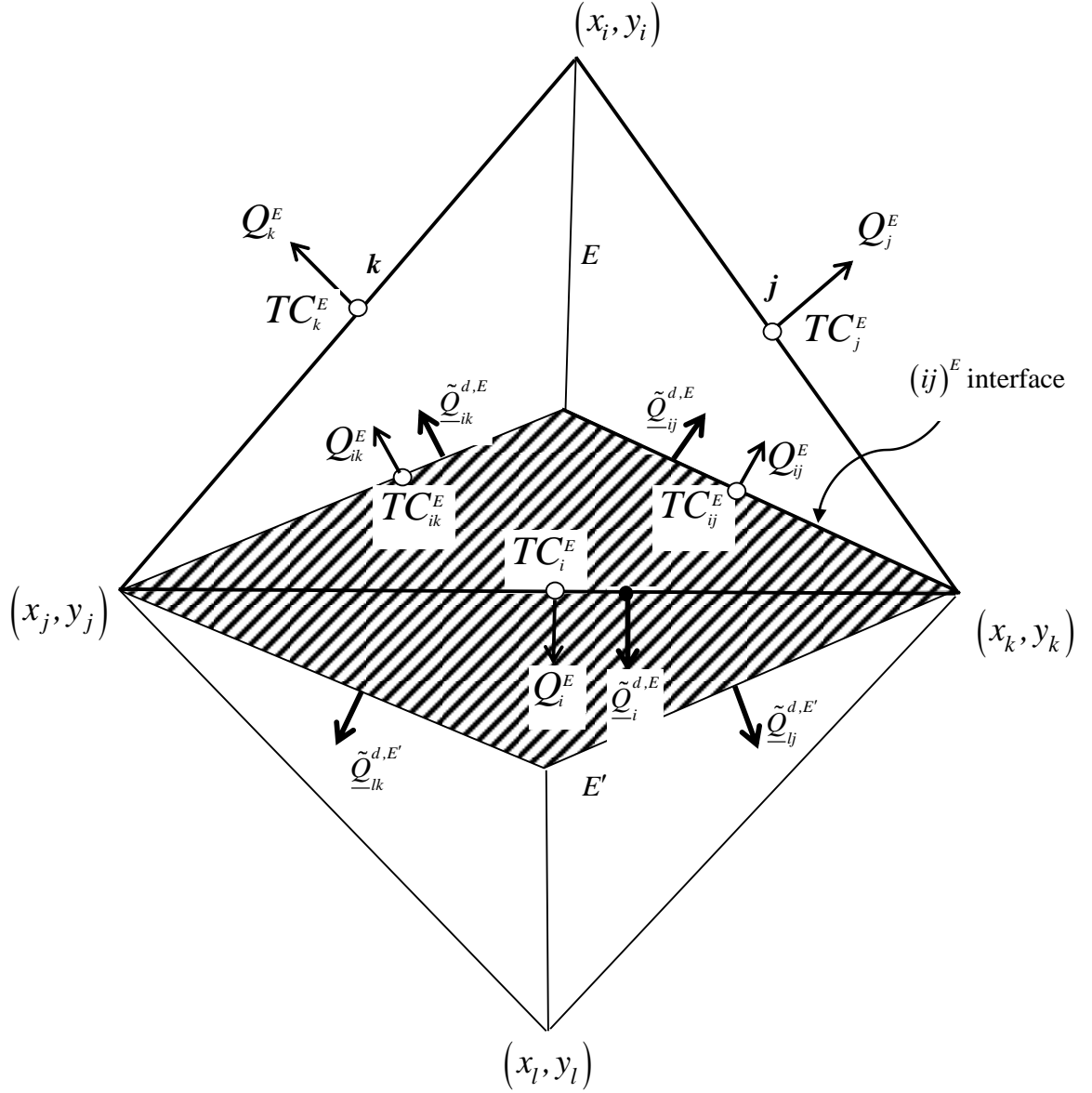
Figure 3: The lumping region $R_i$ associated with the edge $i$, sharing the elements $E$ and $E'$ and formed by the two simplex regions $S_i^E$ and $S_i^{E'}$.

Associating the edge concentration $TC_i^E$ to $R_i$ (see Figure 3 for notations), Eq. (29) gives

$$\left\{ \frac{|E|}{3} \theta_E \frac{\partial TC_i^E}{\partial t} + \underline{\tilde{Q}}_{ij}^{d,E} + \underline{\tilde{Q}}_{ik}^{d,E} \right\} + \{\ \}' = 0 \tag{30}$$

in which $\underline{\tilde{Q}}_{ij}^{d,E}$ and $TC_{ij}^E$ are respectively the dispersive flux and the concentration at the interior interface $(ij)^E$ between the simplex regions $S_i^E$ and $S_j^E$. The shortcut $\{\ \}'$

15

301    designates the same contribution as $\{\ \}$, but of the adjacent element $E'$, in the case of Eq.

302    (30), it corresponds to $\dfrac{|E'|}{3} \theta_{E'} \dfrac{\partial TC_i^E}{\partial t} + \underaccent{\tilde}{Q}_{ij}^{d,E'} + \underaccent{\tilde}{Q}_{ik}^{d,E'}$ .

303    Besides, applying the steady-state dispersive transport Eq. (26) on the simplex region $S_i^E$

304    yields:

305    $$\underaccent{\tilde}{Q}_{ij}^{d,E} + \underaccent{\tilde}{Q}_{ik}^{d,E} + \underaccent{\tilde}{Q}_{i}^{d,E} = 0 \tag{31}$$

306    Finally, substituting Eq. (28) and Eq. (31) into the transport Eq. (30) give the final system

307    to solve with the lumped hybrid MFE scheme:

308    $$\left\{ \dfrac{|E|}{3} \theta_E \dfrac{\partial TC_i^E}{\partial t} + \sum_j \left( \tilde{B}_{i,j}^{E,-1} - \dfrac{\tilde{\alpha}_i^E \tilde{\alpha}_j^E}{\tilde{\alpha}^E} \right) TC_j^E \right\} + \{\ \}' = 0 \tag{32}$$

309    Note that

310    1. The lumped hybrid formulation Eq. (32) and the standard hybrid formulation (Eqs (24)-

311       (25)) are exactly the same in the case of steady state diffusion transport.

312    2. In the lumped formulation Eq (32), the term of mass (with time derivative) has a

313       contribution only on the diagonal term of the final system matrix. This improves the

314       monotonous character of the solution (see Younes *et al.*, 2006). For instance, in the case

315       of an acute triangulation, the maximum principle is respected by the lumped

316       formulation Eq. (32) whatever the heterogeneity of the porous medium (Younes *et al.*,

317       2006).

318    3. Contrarily to the standard hybrid-MFE scheme, where the discretization of the temporal

319       derivative performed in Eq. (14) was necessary to obtain the final system given by Eq.

320       (18), the lumped scheme given by Eq. (32) keeps the time derivative continuous which

321       allows the use of efficient high order temporal discretization methods via the MOL.

322    4. In the case of 2D triangular elements, the lumped formulation Eq. (32) is algebraically

323       equivalent to the nonconforming Crouzeix-Raviart (Crouzeix and Raviart, 1973) finite

16

324     element method (see Younes *et al.*, 2008). The nonconforming Crouzeix-Raviart

325     method uses the chapeau functions as basis functions to approximate the concentration,

326     like the standard finite element method, but seed nodes are the midpoints of the edges.

## 4. The new upwind-hybrid MFE scheme for advection-dispersion transport

327

328   To avoid the rough approximation (21), we develop hereafter a new upwind-MFE scheme

329   where the advection term is calculated using upwind edge concentration instead of upwind

330   mean concentration of the element *E*. The idea of the scheme is to extend the lumped hybrid-

331   MFE procedure to transport by both advection and dispersion and to use an upwind edge

332   centered FV scheme to avoid unphysical oscillations caused by the hyperbolic nature of

333   advection.

334   The integration of the whole mass conservation Eq. (5) over the lumping region $R_i$ writes:

335
$$\int_{R_i} \theta \frac{\partial C}{\partial t} + \int_{R_i} \nabla.\left(\boldsymbol{q}C\right) + \int_{R_i} \nabla.\tilde{\boldsymbol{q}}_d - \int_{R_i} C\nabla.\boldsymbol{q} = 0 \tag{33}$$

336   Using notations of Figure 3, we obtain

337
$$\left\{ \frac{|E|}{3}\theta_E \frac{\partial TC_i^E}{\partial t} + Q_{ij}^E TC_{ij}^E + Q_{ik}^E TC_{ik}^E + \underline{\tilde{Q}}_{ij}^{d,E} + \underline{\tilde{Q}}_{ik}^{d,E} - TC_i^E\left(Q_{ij}^E + Q_{ik}^E\right)\right\} + \left\{\ \ \right\}' = 0 \tag{34}$$

338   in which $Q_{ij}^E$ is the water flux at the interior interface $\left(ij\right)^E$, evaluated using the RT0

339   approximation of the velocity given by Eq. (6), which yields

340
$$Q_{ij}^E = \frac{1}{3}\left(Q_j^E - Q_i^E\right) \tag{35}$$

341   Using Eq (28) and Eq. (31) and denoting $\lambda_E = \theta_E \dfrac{|E|}{3}$, Eq. (34) becomes

342
$$\left\{ \lambda_E \frac{\partial TC_i^E}{\partial t} + \sum_j \left( \tilde{B}_{i,j}^{E,-1} - \frac{\tilde{\alpha}_i^E \tilde{\alpha}_j^E}{\tilde{\alpha}^E}\right) TC_j^E + Q_{ij}^E TC_{ij}^E + Q_{ik}^E TC_{ik}^E - \left(Q_{ij}^E + Q_{ik}^E\right) TC_i^E \right\} + \left\{\ \ \right\}' = 0 \tag{36}$$

343 The interior concentration $TC_{ij}^E$ at the interface between the simplex regions $S_i^E$ and $S_j^E$ is

344 calculated using an upwind scheme (See Figure 3) defined by:

$$TC_{ij}^E = \tau_{ij}^E TC_i^E + \left(1 - \tau_{ij}^E\right) TC_j^E \tag{36}$$

346 with $\tau_{ij}^E = 1$ if $\left(Q_{ij}^E \geq 0\right)$, else $\tau_{ij}^E = 0$

347 Thus, the final system to solve becomes,

$$\left\{ \lambda_E \frac{\partial TC_i^E}{\partial t} + \sum_j \left( \tilde{B}_{i,j}^{E,-1} - \frac{\tilde{\alpha}_i^E \tilde{\alpha}_j^E}{\tilde{\alpha}^E} \right) TC_j^E + Q_{ij}^E \left(1 - \tau_{ij}^E\right)\left(TC_j^E - TC_i^E\right) + Q_{ik}^E \left(1 - \tau_{ik}^E\right)\left(TC_k^E - TC_i^E\right) \right\}$$

$$+ \{\ \}' = 0$$

349 $\qquad\qquad\qquad\qquad\qquad\qquad\qquad\qquad\qquad\qquad\qquad\qquad\qquad\qquad\qquad$ (37)

350 In the case of a first-order Euler implicit time discretization, Eq. (37) becomes

$$\left\{ \sum_j \left( \tilde{B}_{i,j}^{E,-1} - \frac{\tilde{\alpha}_i^E \tilde{\alpha}_j^E}{\tilde{\alpha}^E} \right) TC_j^{E,n+1} + \lambda_E TC_i^{E,n+1} + Q_{ij}^E \left(1 - \tau_{ij}^E\right)\left(TC_j^{E,n+1} - TC_i^{E,n+1}\right) \\ + Q_{ik}^E \left(1 - \tau_{ik}^E\right)\left(TC_k^{E,n+1} - TC_i^{E,n+1}\right) - \lambda_E TC_i^{E,n} \right\} + \{\ \}' = 0 \quad (38)$$

352 where $\lambda_E = \theta_E \dfrac{|E|}{3\Delta t}$.

353 It is easy to see that, due to upwinding, the system matrix corresponding to Eq. (38) is always

354 an *M*-matrix (a non singular matrix with $m_{ii} > 0$, $m_{ij} \leq 0$) in the case of transport by advection.

355 The *M*-matrix property insures the stability of the scheme since it guaranties the respect of the

356 discrete maximum principle *i.e.* local maxima or minima will not appear in the $C$ solution in

357 a domain without local sources or sinks.

358 Further, Eq. (37) expresses the total exchange between $E$ and $E$' and therefore reflects the

359 continuity of the total advection-dispersion flux between them. Both advective and dispersive

360 fluxes are continuous between the adjacent elements $E$ and $E$'. The advective flux, calculated

361 using the upwind edge concentration, is uniquely defined at the interface of the lumping

362 region and is therefore continuous. As a consequence, the dispersive flux is also continuous

18

363    between $E$ and $E$' since the total flux is continuous at the interface between them.

## 5. Numerical Experiments

365    In this section, a first test case dealing with transport in saturated porous media is simulated

366    with the standard hybrid-MFE and the new upwind-MFE schemes. The results are compared

367    against an analytical solution in order to validate the new developed scheme and to show its

368    robustness for solving advection-dominated transport problems compared to the standard one.

369    The second test case deals with transport in the unsaturated zone and aims to investigate the

370    robustness of the new scheme when combined with the MOL for solving highly nonlinear

371    problems.

**5.1 Transport in saturated porous media: comparison against a 2D analytical solution**

373    The hybrid and upwind MFE formulations are compared against the analytical solution

374    developed by Leij and Dane (1990) for a simplified 2D transport problem (Figure 4). The test

375    case has been employed by Putti *et al.* (1990) and Siegel *et al.* (1997) for the verification of

376    transport codes. It deals with the contamination from the left boundary of a 2D rectangular

377    domain of dimension $(0,100) \times (0,40)$.
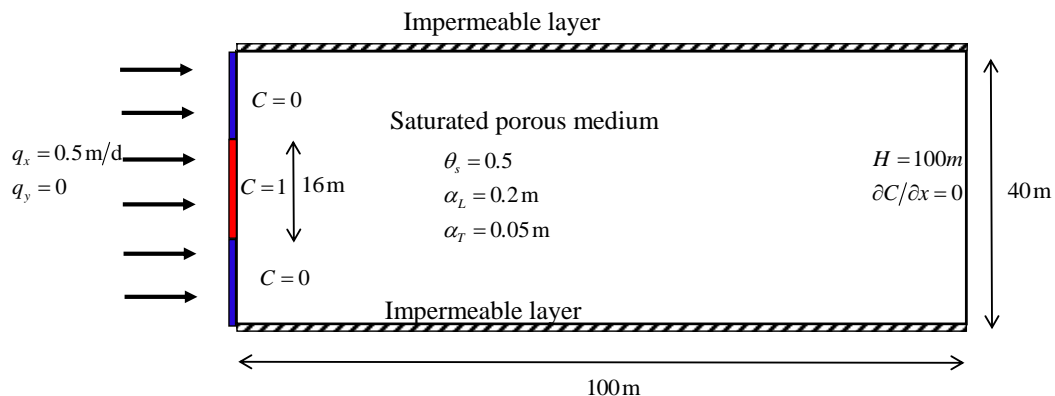


379    Figure 4: Description of the problem of the contamination of a 2D saturated porous medium.

380    The boundary conditions for the transport are of Dirichlet type at the inflow (left vertical

381    boundary), with

19

$$
382 \qquad C = \begin{cases} 0 & \text{for } x = 0 \text{ and } 0 \le y < 12 \\ 1 & \text{for } x = 0 \text{ and } 12 \le y \le 28 \\ 0 & \text{for } x = 0 \text{ and } 28 < y \le 40 \end{cases} \qquad (39)
$$

383    A zero diffusive flux is imposed at the right vertical outflow boundary. The top and bottom

384    are impermeable boundaries. A uniform horizontal flow occurs from left to right with a

385    constant flux $q_x = 0.5$ m/day prescribed at the left vertical boundary and a fixed head

386    $H = 100$ m at the right vertical boundary. The longitudinal and transverse dispersivities are

387    $\alpha_L = 0.2m$ and $\alpha_T = 0.05m$, respectively. The domain is discretized with a fine unstructured

388    triangular mesh formed by 33216 elements, and the simulation is performed for a final

389    simulation time T = 30 days using the Euler-implicit time discretization with a fixed time step

390    of 0.1 day. The linear systems are solved in each time step with a direct solver using an

391    unsymmetric-pattern multifrontal method and a direct sparse LU factorization (UMFPACK).

392    The analytical solution of this test case for an infinite domain is given by Leij and Dane

393    (1990):

$$
394 \qquad C_{analy}(x,y,t) = \frac{x}{(16\pi\alpha_L)^{1/2}} \int_0^T \tau^{-3/2} \left\{ erf\left[ \frac{y-12}{(4\alpha_T\tau)^{1/2}} \right] + erf\left[ \frac{28-y}{(4\alpha_T\tau)^{1/2}} \right] \right\} exp\left[ -\frac{(x-\tau)^2}{4\alpha_L\tau} \right] d\tau \quad (40)
$$

395    with $erf(x) = \dfrac{2}{\sqrt{\pi}} \int_0^x exp(-\tau^2) d\tau$.

396

397    The final distributions of the concentration with both hybrid-MFE and upwind-MFE schemes

398    are depicted in Figure 5. Although we have used an unstructured mesh, the two schemes yield

399    almost symmetrical results. The hybrid-MFE scheme (Figure 5a) yields a solution with

400    unphysical oscillations. Indeed, around 1.2 % of the contaminated region (*i.e.* the region with

401    $|C| \ge 10^{-5}$) exhibits unphysical oscillations with 0.4 % of the contaminated region with

402    $C \le -10^{-3}$ and 0.8 % of the contaminated region with $C \ge 1.001$. These unphysical

403    oscillations, although they seem moderate, can be dramatic, for instance, when dealing with

404    reactive transport where some reactions occur only if the concentration excesses a certain

405    threshold. The solution obtained with the new upwind formulation (Figure 5b) is monotone

406    (all concentrations are between 0 and 1) which is in agreement with the physics. However,

407    these results come at the expense of some numerical diffusion added to the solution. To

408    appreciate the quality of both solutions and validate the upwind-MFE method, we compare

409    the concentration profile of the two methods to the analytical solution of Leij and Dane (1990)

410    for a horizontal section located at y = 20 m and a vertical section located at x = 20 m.

411
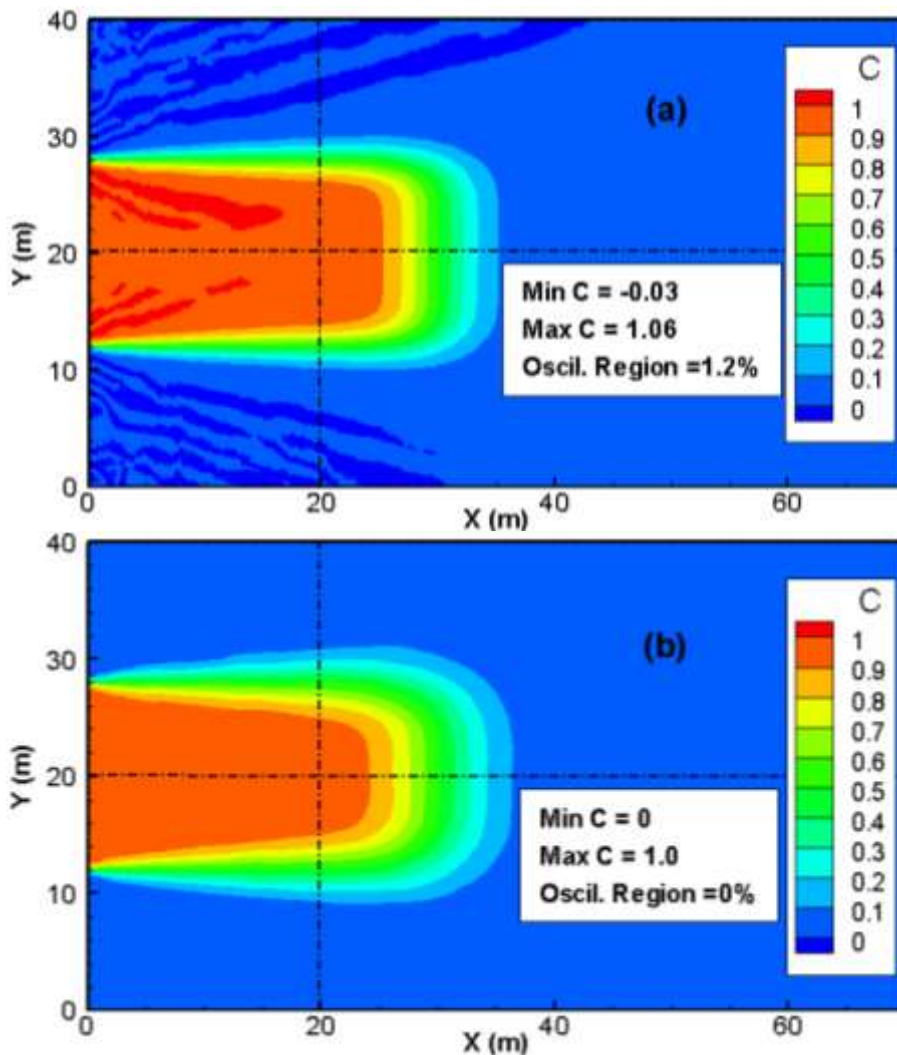
412

413



414    Figure 5: Concentration distribution with the hybrid-MFE and the upwind-MFE methods for

415             the 2D saturated transport problem (only the region $x \leq 70\,\text{m}$ is depicted).

416

417  The results of figure 6 show that the solution of both hybrid-MFE and upwind-MFE methods

418  are in very good agreement with the analytical solution, which validates the new upwind-

419  MFE numerical model. Note, however, that a small numerical diffusion is observed with the

420  upwind-MFE solution, which is especially visible in figure 6b. Indeed, for the simulated

421  problem, the transverse dispersivity is much smaller than the longitudinal one, and, as a

422  consequence, the concentration front is sharper in the vertical section than in the horizontal

423  one. This explains why the numerical diffusion generated by the upwind-MFE method is

424  more pronounced in Figure 6b than in Figure 6a.

425
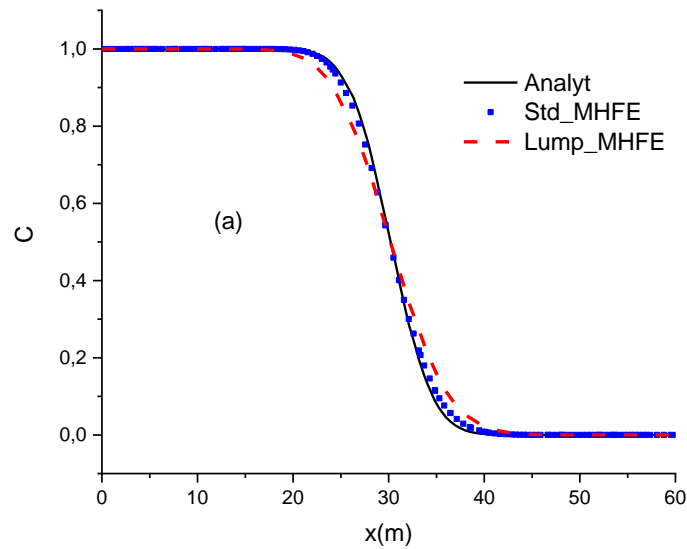
426
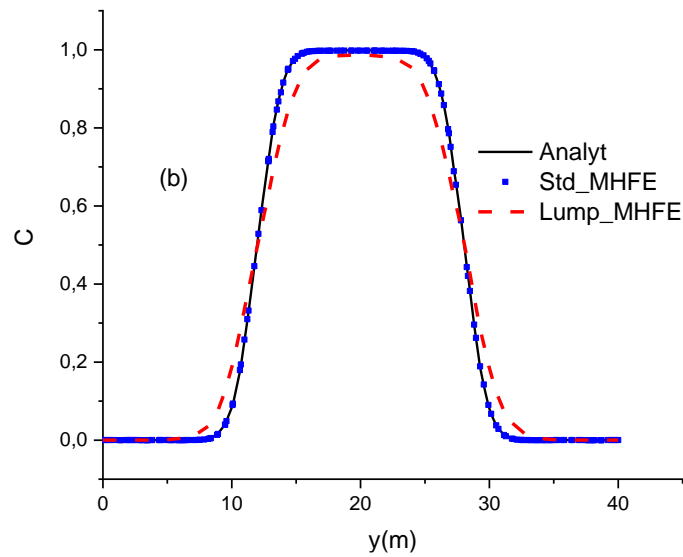


427

428    Figure 6: Concentration profiles at y = 20m (a) and x = 20 m (b) with the analytical, hybrid-

429    MFE and upwind-MFE solutions.

430    The test problem is then simulated using different mesh refinements to investigate the order of

431    convergence of the new method. We start with a uniform mesh formed by 1000 triangles and

432    a time step $\Delta t = 0.1s$. In each level of refinement, each triangle is subdivided into four similar

433    triangles, by joining the three mid-edges and the time step $\Delta t$ is halved. The following error

434    is computed (Brunner *et al.*, 2014):

435
$$Er = \left\{ \left\| C_{analyt}\left(t^N\right) - C\left(t^N\right) \right\|_0^2 + \Delta t \sum_{n=1}^{N} \left\| \tilde{\boldsymbol{q}}_{analyt}^t\left(t^n\right) - \tilde{\boldsymbol{q}}^t\left(t^n\right) \right\|_0^2 \right\}^{1/2} \tag{39}$$

436    where $\tilde{\boldsymbol{q}}^t = \tilde{\boldsymbol{q}}_a + \tilde{\boldsymbol{q}}_d$ is the total advection-dispersion flux and $N$ the total number of time

437    steps.

438    The runs are performed on a single computer with an Intel Xeon E-2246G processor and 32

439    GB memory. The results of the computations, summarized in Table 1, clearly show optimal

440    first order convergence in space and time for the developed upwind-hybrid MFE method.

| Ref. level | # unknowns | Error $Er$ | Reduction | CPU time (s) |
|:---:|:---:|:---:|:---:|:---:|
| 1 | 1535 | 2.55 | | 4.9 |
| 2 | 6070 | 1.296 | 1.97 | 38.6 |
| 3 | 24140 | 0.655 | 1.98 | 272 |
| 4 | 96280 | 0.329 | 1.99 | 2068 |
| 5 | 384560 | 0.165 | 2.00 | 16567 |

441    Table 1: Numerical results for the new upwind-hybrid MFE method.

442    **5.2 Transport in a variably-saturated porous medium**

443    In this test case, the developed upwind-MFE method is combined with the MOL for solving

444    contaminant transport in a variably-saturated porous medium. The advection-dispersion

445    equation is transformed to an Ordinary Differential Equation (ODE) using the new upwind-

446    MFE formulation for the spatial discretization, whereas the time derivative is maintained

447    continuous. Therefore, high-order time integration methods included in efficient ODE solvers

448    can be employed. With these solvers, both the time step size and the order of the time

449    integration can vary during the simulation to deliver accurate results in an acceptable

450    computational time.

451    To investigate the robustness and efficiency of the combination of the developed upwind-

452    MFE method with the MOL, we simulate in this section the problem of contaminant

453    infiltration into a variably-saturated porous medium.
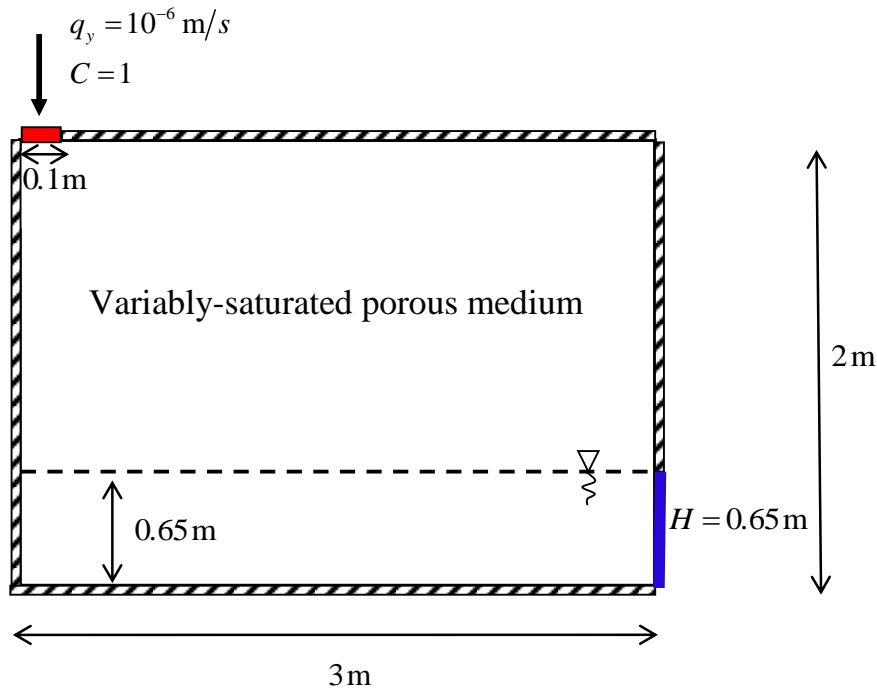


454

455    Figure 7: Description of the problem of contaminant infiltration into a 2D variably-saturated

456    porous medium.

457

458    The domain (Figure 7) is a rectangular box of 3m × 2m, filled with sand, with an initial water

459    table at 0.65m and hydrostatic pressure distribution. An infiltration of a tracer contaminant is

460    applied over the left-most 0.1m of the surface with a constant flux of $10^{-6}\,\text{m/s}$. The right

461    vertical side has a fixed head $H = 0.65\,\text{m}$ below the water table and an impermeable boundary

462    above it. The left vertical side as well as the upper (except the infiltration zone) and bottom

463    boundaries are impermeable boundaries.

464    In this problem, the flow and transport are coupled by the velocity, which is obtained by

465    solving the following pressure-head form of the nonlinear Richards' equation:

466
$$\left(c(h)+S_S\frac{\theta}{\theta_S}\right)\frac{\partial H}{\partial t}+\nabla\cdot\boldsymbol{q}=0 \tag{40}$$

467
$$\boldsymbol{q}=-k_r\boldsymbol{K}\nabla H \tag{41}$$

468    with $S_S$ the specific mass storativity related to head changes [L$^{-1}$], $H=h+y$ the equivalent

469    head [L], $h=\dfrac{P}{\rho g}$ the pressure head, $P$ the pressure [Pa], $\rho$ the fluid density [ML$^{-3}$], $g$ the

470    gravity acceleration [LT$^{-2}$], $y$ the upward vertical coordinate [L], $c(h)$ the specific moisture

471    capacity [L$^{-1}$], $\theta_S$ the saturated water content [L$^3$L$^{-3}$], $\boldsymbol{q}$ the Darcy velocity [LT$^{-1}$],

472    $\boldsymbol{K}=\dfrac{\rho g}{\mu}\boldsymbol{k}$ the hydraulic conductivity [LT$^{-1}$], $\boldsymbol{k}$ the permeability [L$^2$], $\mu$ the fluid dynamic

473    viscosity [ML$^{-1}$T$^{-1}$] and $k_r$ the relative conductivity [-].

474    We use the standard van Genuchten (1980) model for the relationship between water content

475    and pressure head:

476
$$S_e=\frac{\theta(h)-\theta_r}{\theta_s-\theta_r}=\begin{cases}\dfrac{1}{\left(1+|\alpha h|^n\right)^m} & h<0\\[2mm] 1 & h\geq 0\end{cases} \tag{42}$$

477    where $\alpha$ [L$^{-1}$] and $n$ [-] are the van Genuchten parameters, $m=1-1/n$, $S_e$ [-] is the effective

478    saturation and $\theta_r$ [-] is the residual water content. The conductivity-saturation relationship is

479    derived from the Mualem (1976) model:

480
$$k_r=S_e^{1/2}\left[1-\left(1-S_e^{1/m}\right)^m\right]^2 \tag{43}$$

481    The material properties of the test problem are given in Table 2.

| Parameters | |
| --- | --- |
| $\theta_r$ | 0.01 |
| $\theta_s$ | 0.3 |
| $\alpha$ (cm$^{-1}$) | 0.033 |
| $n$ | 4.1 |
| $K$ (cm/s) | $10^{-2}$ |
| $S_s$ (cm$^{-1}$) | $10^{-10}$ |
| $D_m$ (m$^2$/s) | $10^{-9}$ |
| $\rho$ (kg/m$^3$) | 1000 |
| $\mu$ (kg/m/s) | 0.001 |

482

483    Table 2: Parameters for the problem of infiltration into a 2D variably-saturated porous

484                                             medium.

485

486    The simulation is performed for 80 hours using a triangular mesh formed by 4273 triangular

487    elements. Two test cases are investigated. In the first test case, the longitudinal and transverse

488    dispersivities are $\alpha_L = 0.03m$ and $\alpha_T = 0.003m$, respectively. The second test case is less

489    diffusive with $\alpha_L = 0.01m$ and $\alpha_T = 0.001m$.

490    The coupled nonlinear flow-transport system is solved using the MOL, which allows the use

491    of efficient high-order time integration methods, for both the hybrid-MFE and the upwind-

492    MFE schemes. To this aim, a hybrid-MFE formulation with continuous time derivative was

493    developed by extending the lumping procedure, developed in Younes *et al*. (2006) for the

494    flow equation, to the advection-dispersion transport Eq. (5).

495    The time integration is performed with the DASPK time solver which uses an efficient

496    automatic time-stepping scheme based on the Fixed Leading Coefficient Backward

497    Difference Formulas (FLCBDF). The linear systems arising at each time step are solved with

498    the preconditioned Krylov iterative method. The nonlinear problem is linearized using the

499    Newton method with a numerical approximation of the Jacobian matrix.

500    The results of the hybrid-MFE and the upwind-MFE methods are depicted in Figure 8 for the

501     first test case involving high dispersion. Good agreement can be observed between the results

502     of the hybrid-MFE (Figure 8a) and upwind-MFE (Figure 8b) schemes when combined with

503     the MOL. In these figures, the contaminant progresses essentially vertically through the

504     unsaturated zone of the soil. When the saturated zone is reached, the contaminant progresses

505     horizontally and remains close to the water table. Note that the results of both schemes are

506     stable and free from unphysical oscillations (Figures 8a and 8b).
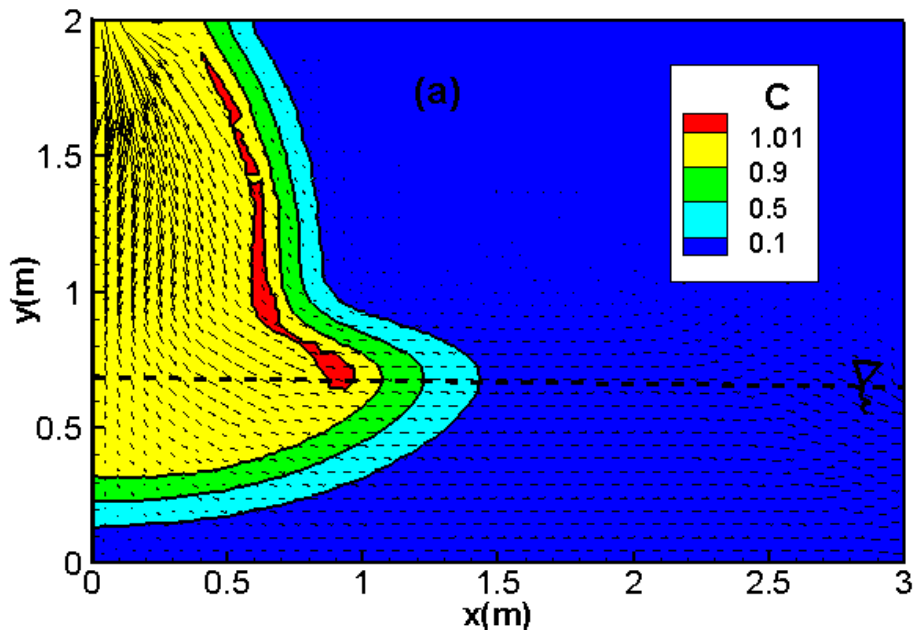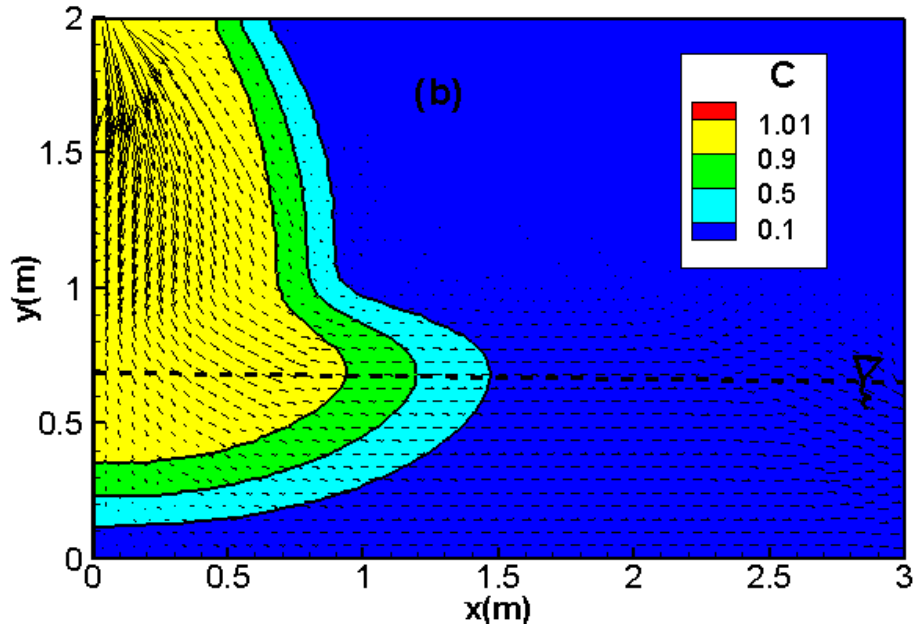
507
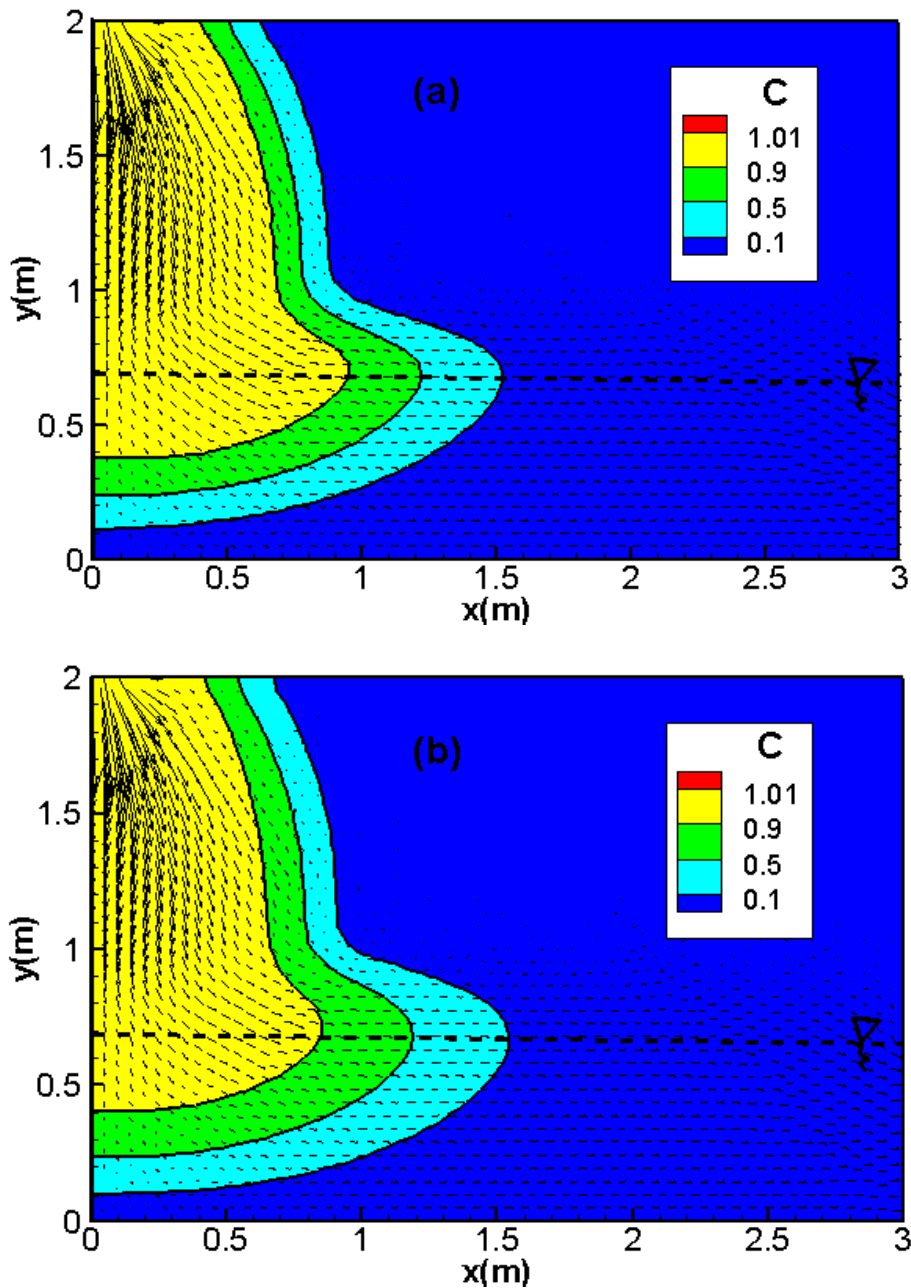


508

509           Figure 8: Concentration distribution, with the hybrid-MFE (a) and the upwind-MFE (b)

510        schemes for the transport problem with high dispersion in a variably-saturated porous

511                             medium.

512    For the second test case with lower dispersion $\left(\alpha_L = 0.01m, \alpha_T = 0.001m\right)$, the hybrid-MFE

513    method yields unstable results containing unphysical oscillations (red color in Figure 9a).

514    These oscillations hamper the convergence of the numerical model, and severe convergence

515    issues can be encountered if we further decrease the dispersivity values. The results of the

516    upwind-MFE scheme are monotone and do not contain any unphysical oscillation (Figure 9b).

517    These results point out the robustness of the new upwind MFE method for transport in

518    saturated and unsaturated porous media. The developed transport scheme has recently been

519    successfully combined with the MFE method for fluid flow to simulate nonlinear flow and

520    transport in unsaturated fractured porous media using the 1D-2D discrete fracture matrix

521    (DFM) approach (Younes et al., 2022b).



522

523

524     Figure 9: Concentration distribution with the hybrid-MFE (a) and upwind-MFE (b) methods

525        for the transport problem with low dispersion in variably-saturated porous medium.

## 6. Conclusion

527
528 MFE is a robust numerical method well adapted for diffusion problems on heterogeneous

529 domains and unstructured meshes. When applied to transport equations, the MFE solution can

530 exhibit strong unphysical oscillations due to the hyperbolic nature of advection. Upwind

531 schemes can be used to avoid such oscillations, although they introduce some numerical

532 diffusion. In this work, we developed an upwind scheme that does not require any

533 approximation for the upwind concentration. The method can be seen as a combination of an

534 upwind edge/face centred FV method with the lumped formulation of the hybrid-MFE

535 method. It ensures continuity of both advective and dispersive fluxes between adjacent

536 elements and allows to maintain the time derivative continuous, which facilitates employment

537 of high order time integration methods via the method of lines (MOL) for nonlinear problems.

538 Numerical simulations for the transport in a saturated porous medium show that the standard

539 hybrid-MFE method can generate unphysical oscillations due to the hyperbolic nature of

540 advection. These unphysical oscillations are completely avoided with the new upwind-MFE

541 scheme. The simulation of the problem of contaminant transport in a variably-saturated

542 porous medium shows that only the upwind-MFE scheme provides a stable solution. The

543 results point out the robustness of the developed upwind-MFE scheme when combined with

544 the MOL for solving nonlinear transport problems.

545

546

547

548

# References

549

550 Belfort, B., Ramasomanana, F., Younes, A., and Lehmann, F.: An Efficient Lumped Mixed
551         Hybrid Finite Element Formulation for Variably Saturated Groundwater Flow, 8, 352–
552         362, https://doi.org/10.2136/vzj2008.0108, 2009.

553 Brezzi, F. and Fortin, M. (Eds.): Mixed and Hybrid Finite Element Methods, Springer New
554         York, New York, NY, https://doi.org/10.1007/978-1-4612-3172-1, 1991.

555 Brezzi, F., Douglas, J., and Marini, L. D.: Two families of mixed finite elements for second
556         order    elliptic    problems,    Numer.    Math.,    47,    217–235,
557         https://doi.org/10.1007/BF01389710, 1985.

558 Brunner, F., Radu, F. A., and Knabner, P.: Analysis of an Upwind-Mixed Hybrid Finite
559         Element Method for Transport Problems, SIAM J. Numer. Anal., 52, 83–102,
560         https://doi.org/10.1137/130908191, 2014.

561 Chavent, G. and Jaffré, J.: Mathematical models and finite elements for reservoir simulation:
562         single phase, multiphase, and multicomponent flows through porous media, North-
563         Holland ; Sole distributors for the U.S.A. and Canada, Elsevier Science Pub. Co,
564         Amsterdam ; New York : New York, N.Y., U.S.A, 376 pp., 1986.

565 Chavent, G. and Roberts, J. E.: A unified physical presentation of mixed, mixed-hybrid finite
566         elements and standard finite difference approximations for the determination of
567         velocities in waterflow problems, 14, 329–348, https://doi.org/10.1016/0309-
568         1708(91)90020-O, 1991.

569 Crouzeix, M., Raviart, P.A. Conforming and nonconforming finite element methods for
570         solving the stationary Stokes equations, R.A.I.R.O. R3, 7, 33-76, 1973.

571 Dawson, C.: Analysis of an Upwind-Mixed Finite Element Method for Nonlinear contaminant
572         Transport    Equations,    SIAM    J.    Numer.    Anal.,    35,    1709–1724,
573         https://doi.org/10.1137/S0036142993259421, 1998.

574 Dawson, C. N. and Aizinger, V.: Upwind mixed methods for transport equations, 3, 93–110,
575         1999.

576 Fahs, M., Younes, A., and Lehmann, F.: An easy and efficient combination of the Mixed
577         Finite Element Method and the Method of Lines for the resolution of Richards'
578         Equation,    Environmental    Modelling    &    Software,    24,    1122–1126,
579         https://doi.org/10.1016/j.envsoft.2009.02.010, 2009.

580 van Genuchten, M. T.: A Closed-form Equation for Predicting the Hydraulic Conductivity of
581         Unsaturated Soils, Soil Science Society of America Journal, 44, 892–898,

https://doi.org/10.2136/sssaj1980.03615995004400050002x, 1980.

Hoteit, H., Mosé, R., Philippe, B., Ackerer, P., and Erhel, J.: The maximum principle violations of the mixed-hybrid finite-element method applied to diffusion equations: Mixed-hybrid finite element method, 55, 1373–1390, https://doi.org/10.1002/nme.531, 2002.

Hoteit, H., Erhel, J., Mosé, R., Philippe, B., and Ackerer, P.: Numerical Reliability for Mixed Methods Applied to Flow Problems in Porous Media, n.d.

Koohbor, B., Fahs, M., Hoteit, H., Doummar, J., Younes, A., and Belfort, B.: An advanced discrete fracture model for variably saturated flow in fractured porous media, 140, 103602, https://doi.org/10.1016/j.advwatres.2020.103602, 2020.

Leij, F. J. and Dane, J. H.: Analytical solutions of the one-dimensional advection equation and two- or three-dimensional dispersion equation, 26, 1475–1482, https://doi.org/10.1029/WR026i007p01475, 1990.

Mazzia, A.: An analysis of monotonicity conditions in the mixed hybrid finite element method on unstructured triangulations, 76, 351–375, https://doi.org/10.1002/nme.2330, 2008.

Mualem, Y.: A new model for predicting the hydraulic conductivity of unsaturated porous media, Water Resour. Res., 12, 513–522, https://doi.org/10.1029/WR012i003p00513, 1976.

Putti, M., Yeh, W.W.-G., and Mulder, W.A.: A triangular finite volume approach with high-resolution upwind terms for the solution of groundwater transport equations, Water Resources Res., 26, 2865-2880, https://doi.org/10.1029/WR026i012p02865, 1990.

Radu, F. A., Suciu, N., Hoffmann, J., Vogel, A., Kolditz, O., Park, C.-H., and Attinger, S.: Accuracy of numerical simulations of contaminant transport in heterogeneous aquifers: A comparative study, Advances in Water Resources, 34, 47–61, https://doi.org/10.1016/j.advwatres.2010.09.012, 2011.

Raviart, P. A. and Thomas, J. M.: A mixed finite element method for 2-nd order elliptic problems, in: Mathematical Aspects of Finite Element Methods, Berlin, Heidelberg, 292–315, 1977.

Siegel, P., Mosé, R., Ackerer, P., and Jaffré, J.: Solution of the Advection Diffusion Equation using a combination of Discontinuous and Mixed Finite Elements, Int. J. Numer. Meth. Fluids, 24: 595-613. https://doi.org/10.1002/(SICI)1097-0363(19970330)24:6<595::AID-FLD512>3.0.CO;2-I, 1997.

Traverso, L., Phillips, T. N., and Yang, Y.: Mixed finite element methods for groundwater flow in heterogeneous aquifers, Computers & Fluids, 88, 60–80, https://doi.org/10.1016/j.compfluid.2013.08.018, 2013a.

Traverso, L., Phillips, T. N., and Yang, Y.: Mixed finite element methods for groundwater flow in heterogeneous aquifers, Computers & Fluids, 88, 60–80, https://doi.org/10.1016/j.compfluid.2013.08.018, 2013b.

Vohralík, M.: A Posteriori Error Estimates for Lowest-Order Mixed Finite Element Discretizations of Convection-Diffusion-Reaction Equations, 45, 1570–1599, https://doi.org/10.1137/060653184, 2007.

Younes, A., Mose, R., Ackerer, P., and Chavent, G.: A New Formulation of the Mixed Finite Element Method for Solving Elliptic and Parabolic PDE with Triangular Elements, 149, 148–167, https://doi.org/10.1006/jcph.1998.6150, 1999.

Younes, A., Ackerer, P., and Lehmann, F.: A new mass lumping scheme for the mixed hybrid finite element method, International Journal for Numerical Methods in Engeneering, 67, 89–107, https://doi.org/10.1002/nme.1628, 2006.

Younes, A., Fahs, M., and Ahmed, S.: Solving density driven flow problems with efficient spatial discretizations and higher-order time integration methods, Advances in Water Resources, 32, 340–352, https://doi.org/10.1016/j.advwatres.2008.11.003, 2009.

Younes, A., Ackerer, P., and Delay, F.: Mixed finite elements for solving 2-D diffusion-type equations, Rev. Geophys., 48, RG1004, https://doi.org/10.1029/2008RG000277, 2010.

Younes, A., Koohbor, B., Belfort, B., Ackerer, P., Doummar, J., and Fahs, M.: Modeling variable-density flow in saturated-unsaturated porous media: An advanced numerical model, Advances in Water Resources, 159, https://doi.org/10.1016/j.advwatres.2021.104077, 2022a.

Younes, A., Hoteit H., Helmig, R., and Fahs, M.: A robust fully mixed finite element model for flow and transport in unsaturated fractured porous media, Advances in Water Resources, Volume 166, https://doi.org/10.1016/j.advwatres.2022.104259, 2022b.